ARMY RESEARCH LABORATORY

Nondestructive Evaluation of Damaged and As-Fabricated Encapsulated Ceramic Panels

by William H. Green, Raymond Brennan, and Robert H. Carter

ARL-TR-4823 **May 2009**

NOTICES

Disclaimers

The findings in this report are not to be construed as an official Department of the Army position unless so designated by other authorized documents.

Citation of manufacturer's or trade names does not constitute an official endorsement or approval of the use thereof.

Destroy this report when it is no longer needed. Do not return it to the originator.

Army Research Laboratory
Aberdeen Proving Ground, MD 21005-5069

ARL-TR-4823 **May 2009**

Nondestructive Evaluation of Damaged and As-Fabricated Encapsulated Ceramic Panels

William H. Green, Raymond Brennan, and Robert H. Carter
Weapons and Materials Research Directorate, ARL

REPORT DOCUMENTATION PAGE	Form Approved OMB No. 0704-0188

1. REPORT DATE *(DD-MM-YYYY)*	2. REPORT TYPE	3. DATES COVERED (From - To)
May 2009	Final	1 January 2008–31 December 2008

4. TITLE AND SUBTITLE
Nondestructive Evaluation of Damaged and As-Fabricated Encapsulated Ceramic Panels

5a. CONTRACT NUMBER

5b. GRANT NUMBER

5c. PROGRAM ELEMENT NUMBER
2182040

6. AUTHOR(S)
William H. Green, Raymond Brennan, and Robert H. Carter

5d. PROJECT NUMBER
AH80

5e. TASK NUMBER

5f. WORK UNIT NUMBER

7. PERFORMING ORGANIZATION NAME(S) AND ADDRESS(ES)
U.S. Army Research Laboratory
ATTN: AMSRD-ARL-WM-MD
Aberdeen Proving Ground, MD 21005-5069

8. PERFORMING ORGANIZATION REPORT NUMBER
ARL-TR-4823

9. SPONSORING/MONITORING AGENCY NAME(S) AND ADDRESS(ES)

10. SPONSOR/MONITOR'S ACRONYM(S)

11. SPONSOR/MONITOR'S REPORT NUMBER(S)

12. DISTRIBUTION/AVAILABILITY STATEMENT
Approved for public release; distribution is unlimited.

13. SUPPLEMENTARY NOTES

14. ABSTRACT
X-ray computed tomography (XCT) and ultrasonic testing (UT) are two major nondestructive evaluation (NDE) methods used to inspect a wide variety of materials and components. Current work in the NDE of materials at the U.S. Army Research Laboratory includes inspection and analysis of individual ceramic targets and ceramic panels. A number of samples have been evaluated using XCT and UT, including encapsulated panels. XCT and UT results from NDE studies of damaged and as-fabricated encapsulated ceramic panels will be shown and discussed. The results from the two NDE methods will be compared and contrasted.

15. SUBJECT TERMS
computed tomography, ultrasonic testing, encapsulated ceramics, damage

16. SECURITY CLASSIFICATION OF:			17. LIMITATION OF ABSTRACT	18. NUMBER OF PAGES	19a. NAME OF RESPONSIBLE PERSON
a. REPORT	b. ABSTRACT	c. THIS PAGE			William H. Green
Unclassified	Unclassified	Unclassified	UU	30	19b. TELEPHONE NUMBER (*Include area code*) 410-306-0817

Standard Form 298 (Rev. 8/98)
Prescribed by ANSI Std. Z39.18

Contents

List of Figures

List of Tables

INTENTIONALLY LEFT BLANK.

1. Introduction

Nondestructive evaluation (NDE) or nondestructive testing is a discipline of materials science that encompasses a wide variety of inspection modalities. NDE is applicable to an extremely wide variety of materials, components, and systems and is utilized to inspect objects at the surface, subsurface, and in the interior. Two methods used for the evaluation and analysis of internal geometrical and physical characteristics of materials are x-ray computed tomography (XCT) and ultrasonic testing (UT) or scanning. Both of these methods have been used to characterize armor ceramics, including ballistically damaged ceramics (*1–5*), and XCT has been used to characterize and evaluate ballistically damaged encapsulated ceramic panels (*6*). Ceramic materials are currently typically combined with other materials in armor panel structures in order to decrease weight without losing ballistic performance. Encapsulated panels in which the ceramic material is enclosed and backed by a supporting material are an example of this approach. Two encapsulated ceramic panel specimens were characterized and evaluated using XCT and, in the case of the second specimen, also characterized using UT.

2. XCT

XCT is broadly applicable to any material or test object through which a beam of penetrating radiation may be passed and detected, including metals, plastics, ceramics, metallic/nonmetallic composite material, and assemblies. The principal advantage of XCT is that it provides densitometric (i.e., radiological density and geometry) images of thin cross sections through an object in a noninvasive manner. Because of the absence of structural superimposition, images are much easier to interpret than conventional radiological images. The user can quickly learn to read XCT data because images correspond more closely to the way the human mind visualizes three-dimensional (3-D) structures than two-dimensional (2-D) projection radiology (i.e., film radiography, real-time radiography, and digital radiography) (7–*10*). Further, because XCT images are digital, the images may be enhanced, analyzed, compressed, archived, input as data to performance calculations, compared with digital data from other nondestructive evaluation modalities, or transmitted to other locations for remote viewing, or a combination thereof (*8*, *9*).

3. UT

Ultrasound NDE uses the transmission of acoustic waves to nondestructively characterize a test specimen (*11–13*). Reflection of these waves is caused by an acoustic impedance mismatch,

which occurs at material boundaries (*11–13*). This can aid in the detection of defects such as pores and inclusions. For C-scan imaging, an ultrasonic transducer is rastered over the desired sample area, and the collected signals from the A-scans, or amplitude scans, are assigned to x and y coordinates. The changes in gated, or selected, reflected amplitude signals are evaluated. In the study described here, the bottom surface reflected signal was gated to study variations and look for distributed effects of inhomogeneities in the bulk of the specimen. The reflected signal amplitude data, given in mV, represented signal gain while the attenuation, given in decibels (dB), represented signal loss. These values were assigned to a color scale or gray scale which represented amplitude changes over the gated regions. The data were mapped according to the assigned scales and the x and y coordinates to produce bulk image maps of the specimen.

4. Description of Specimens and Digital Radiography Scans

The first encapsulated specimen was an ~207-mm (8.1 in) × 361-mm (14.2 in) rectangular section from a larger fully penetrated, impacted test panel. The specimen included a complete penetration and the surrounding area as well as undamaged material farther away. The backing material was not present on the specimen as received. Figure 1 shows photographs of the first specimen with its detached backing material. The second specimen was an ~180-mm (7.1 in) × 210-mm (8.25 in) rectangular section from a larger nonimpacted test panel. The physical sectioning process may have resulted in cracking in the ceramic material of the specimen. Cracking in the ceramic material is visible in the exposed sectioned side of the specimen. Digital radiographs (DRs) of each specimen were taken through their thickness using the 420-keV x-ray tube and linear detector array (LDA) setup in centered rotate-only (RO) mode. The x-ray technique (parameters) of the DRs of the first and second specimen were 405 keV/2.0 mA and 400 keV/2.0 mA, respectively, and geometries of source-to-object distance (SOD) = 750.00 mm and source-to-image distance (SID) = 940.00 mm. Figure 2 shows digital radiographs of each specimen. The two DRs of the first specimen (figures 2a and b) have been processed or "windowed" to accentuate one or some features over others. In the first image, the damage itself immediately around and farther away from what is left of the penetration cavity is emphasized, as is the damage in the ceramic tiles below the penetrated tile. It also shows the tile layup very clearly. In the second image, the actual perimeter of the entrance hole of the penetration cavity itself is emphasized, showing only relatively thin material left intact at the edges and making the rest of the image significantly lighter. The diameter of the entrance of the penetration cavity is ~60 mm. The cracking in the second specimen is not apparent in figure 2c, which is at a larger scale. The sectioned side of the specimen is on the left, and the two horizontal features are visible on the surface of the specimen.

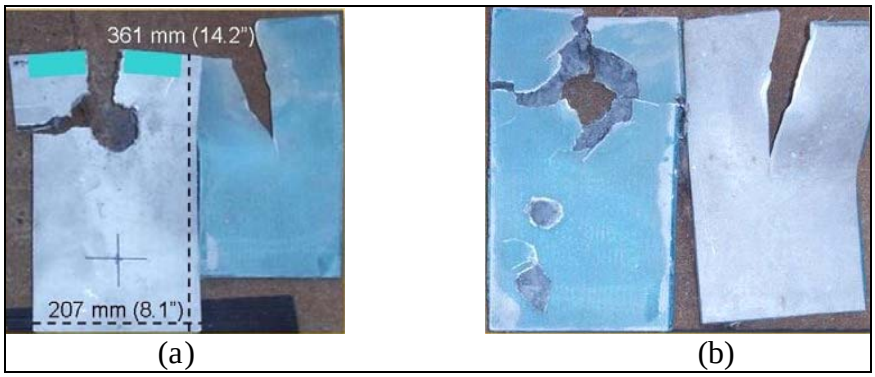

Figure 1. (a) Front and (b) back photographs of the ballistically damaged specimen with the detached titanium backing next to it (on the right in both images). The upper left section in (a) has fractured away from the rest of the panel and is not included in the x-ray evaluation.

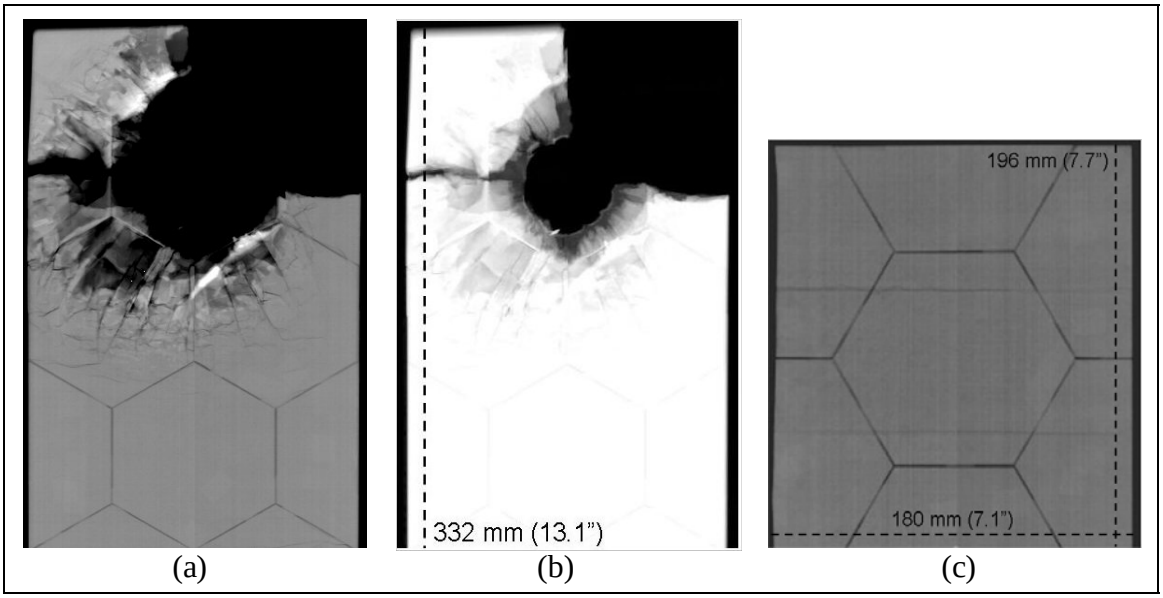

Figure 2. Digital radiographs of both specimens: (a) image emphasizing damage and tile layup, (b) penetration cavity in ballistically damaged specimen, and (c) as-fabricated and sectioned specimen (larger scale).

5. XCT and UT Scanning Procedures

A preliminary series of XCT scans incrementally spaced by 20.00 mm were taken at the bottom to the top of the first specimen. The specimen was held with its faces in a vertical orientation by a portable vice for scanning. Thus, the specimen faces were perpendicular to the horizontal x-ray (collimated) fan beam, resulting in through-thickness, cross-sectional computed tomography (CT) images. The vice was suitably stabilized on the scanning turntable. The

middle of the penetration cavity was at a vertical position of ~288 mm. The vertical scan positions were based on multiples of 20.00 mm below, above, and including the 288.00 position. The undamaged bottom (edge) of the specimen was at a vertical position of about 20 mm, and the top position of the remaining upper portion was at about 381 mm. The specimen was scanned using the 420 keV x-ray tube and LDA setup in offset RO mode. The slice thickness was 0.500 mm, and each slice was reconstructed to a 1024 × 1024 image matrix. The field of reconstruction (FOR) diameter was 230.00 mm. The tube energy and current used were 405 keV and 2.0 mA, respectively, and the focal spot was 0.80 mm. The SOD and SID were 750.00 and 940.00 mm, respectively. The first series of scans were done to get a good understanding of the overall changes in damage features throughout the specimen. A second set of scans was done starting below the penetration cavity and ending within the penetration cavity. These scans were vertically overlapping, with a slice thickness and increment of 0.500 and 0.450 mm, respectively. This was the majority of the slice (image) data analyzed using 3-D solid and point cloud visualization.

Several sets of XCT scans were taken of the second specimen. This resulted in an overall collection of scans incrementally spaced by 5.00 mm starting at the vertical position of the specimen just above the top of the vice. The second specimen was also fixed and held with its faces vertical relative to the scanning turntable like the first specimen. Three sets of overlapping scans were taken in particular sections of interest between vertical positions of 97.00 and 122.20 mm, 125.00 and 148.40 mm, and 182.00 and 206.30 mm. The slice thickness of all the scans was 1.000 mm, and the slice increment of the overlapping scans was 0.900 mm. The bottom (edge) of the specimen was at a vertical position of about 54 mm, and the position of the top was at about 264 mm. Each slice was reconstructed to a 1024 × 1024 image matrix, and the FOR diameter was 195.00 mm. The tube energy and current used were 400 keV and 2.0 mA, respectively, and the focal spot was 0.80 mm. The SOD and SID were 750.00 and 940.00 mm, respectively.

The second specimen was also ultrasonically scanned using a pulse-echo immersion (water) setup. Frequencies of 1, 5, 10, and 15 MHz were used in the scans. Amplitude difference C-scans gated to show the bulk characteristics of the specimen through its thickness were taken at 5 and 10 MHz. The 5- and 10-MHz transducers used for this study were a Panametrics V307 broadband type with a 25.4-mm (1.00-in)-diameter element size and a 215.9-mm (8.50-in) spherical point focus and a Panametrics V315 broadband type with a 19.05-mm (0.75-in)-diameter element size and 163.8-mm (6.45-in) spherical point focus, respectively. The acoustic signals reflected from the top and bottom surfaces of the specimen were selected, or gated. The amplitude of these individual gated signals was measured in addition to measuring the amplitude difference between the gates. The time-of-flight (TOF) was also measured by calculating the difference in milliseconds between the top and bottom surface gated signals. Using a step size of ~0.25 mm (0.01 in), the amplitude and TOF variations were collected and mapped over the area

of the specimen (210 × 180 mm) to look for acoustic variations in the bulk, at each rastered location that represented defects or inhomogeneities (*11*, *12*).

6. Evaluation of Ballistically Damaged Specimen (Specimen 1)

6.1 CT Scans

Figure 3 shows a series of CT scans (images) of the specimen starting at a vertical position of 148.10 mm (figure 3a). The scans in figures 3b–j were taken at vertical positions of 167.90 (figure 3b), 188.15, 207.95, 228.20, 248.00, 251.15, 262.85, 288.00, and 308.00 mm, respectively. The darker vertical bands in these images are indications of the area between adjacent tiles. The slightly darker oblong feature with a somewhat crosshatched appearance in the middle of some of the images (lower heights) is an image artifact. It is not an indication of a real physical feature in the specimen. Damage is clearly evident in the top, or back (exit), side of the specimen at 148.10 mm. There is very slight cracking as far away from the center of the penetration cavity as 160 mm, at a scan height of 128.00 mm. The damage is significantly more severe at 167.90 mm, with connected cracking over most of the width of the specimen towards the back side. Cracks are also present in the middle thickness region of the specimen. Multiple cracks are near and adjacent to the bottom, or front (impact), side of the specimen at 188.15 mm (figure 3c), about 100 mm from the center of the penetration cavity. Braking up of some of the ceramic into rubble as well as bulge in the back face is also present at this height. The amount of rubble is higher with relatively large pieces, and the bulging is more severe at 207.95 mm (figure 3d). The ceramic material is clearly cracked through from the front to the back. Both the front and back side parts of the encapsulant (case) are also cracked, with multiple cracks in the front. The distance between the outer cracks in the front part of the case is about 81 mm. At 228.20 mm (figure 3e) and about 60 mm from the center of the penetration cavity, the rear part of the case is blown open and peeled back. The distance between the two cracks in the front part of the case is about 25 mm. Secondly, at least half of the thickness of the ceramic material no longer has any structural integrity.

At 248.00 mm (figure 3f), the rear of the case is peeled back more, and there is no ceramic material in the center area between the front and the back of the specimen. The front of the case is also on the verge of being penetrated with a major crack. At 251.15 mm (figure 3g), the case and ceramic material have been completely penetrated, with some residual penetrator material (white) just above and to the right of the hole in the front of the case. The hole in the front of the case and the penetration cavity are larger at 262.85 mm (figure 3h), about 25 mm from the center of the penetration cavity. There is not very much material left at 288.00 mm (figure 3i), the scan height of the approximate center of impact. Essentially, very little is still intact at this height, including the missing part of the specimen in the left-hand side of the image. Physically, this is

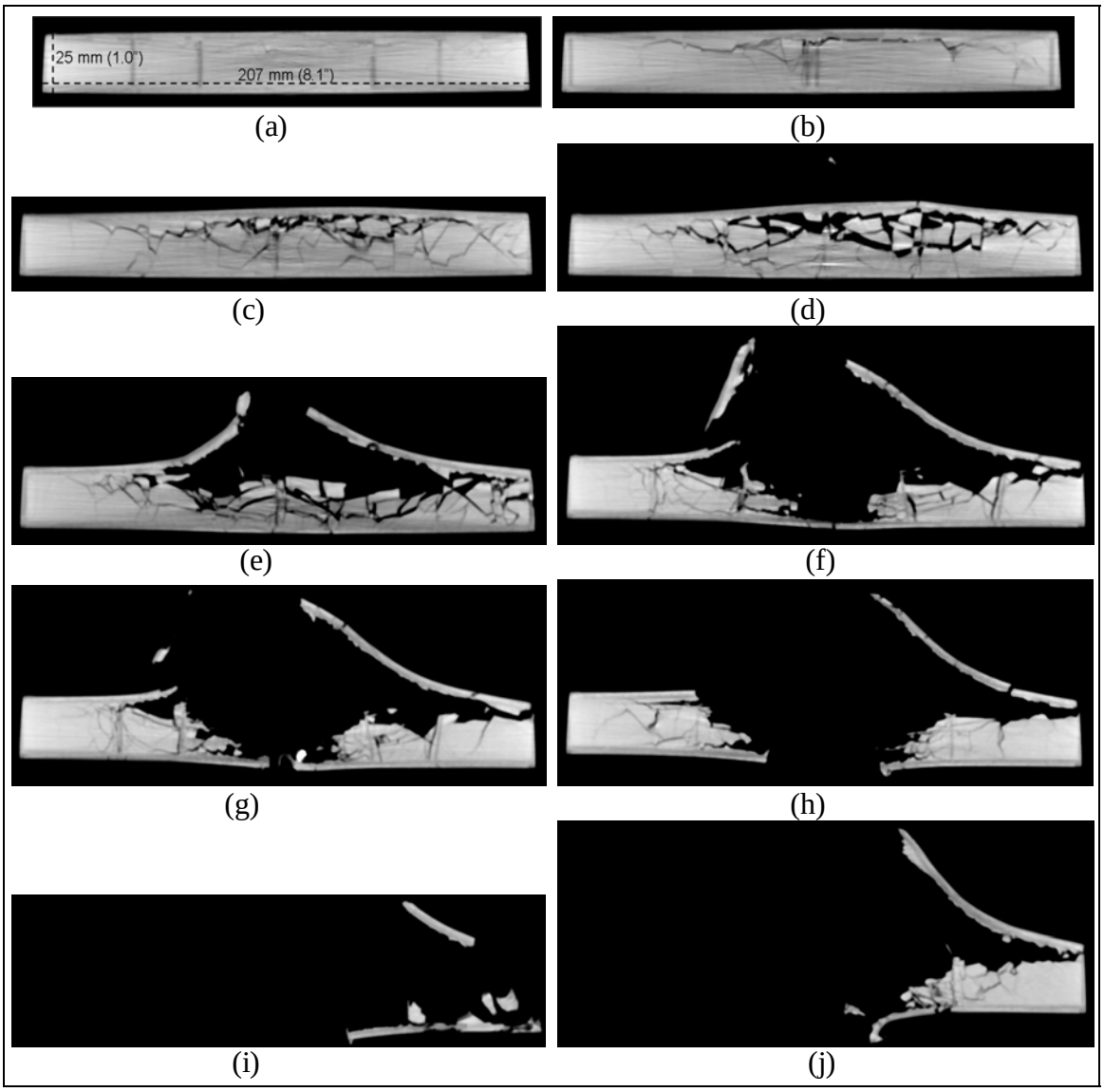

Figure 3. A series of cross-sectional CT scans (images). Scans (a–j) were taken at vertical positions of 148.10, 167.90, 188.15, 207.95, 228.20, 248.00, 251.15, 262.85, 288.00, and 308.00 mm, respectively.

the right-hand side of the specimen as viewed looking at the exit side from the x-ray source perspective (see figure 2). At 288.00 mm and higher, the right-hand side of the specimen is missing because it was blown off by the impact; the image at 308.00 mm (figure 3j) just shows the remaining side.

6.2 Three-Dimensional Solid Visualization

The excellent dimensional accuracy and the digital nature of XCT images allow the accurate volume reconstruction of multiple adjacent or overlapping slices. A virtual 3-D solid image is created by electronically stacking the XCT images, which have a defined thickness over their cross sections (i.e., voxels). These XCT images are stacked one on top of the previous from the

bottom to the top of the specimen or scanned height to generate the 3-D solid image's virtual volume. The 3-D solid images of the specimen were created using the second set of overlapping scans from 140.00 to 265.55 mm high. Figure 4 shows a series of 3-D solid images of the scanned volume with sections virtually removed in (figures c–f). The method of virtual sectioning, which is essentially only showing a portion of each scan, allows viewing of generated surfaces anywhere in the scanned volume in 3-D space. The view in figure 4 is looking at the front of the specimen tilted forward, except for figure 4b, which is looking at the back of the specimen with that side tilted forward. Figures 4a and b show the entire scanned volume, with surfaces and no sections virtually removed. Figure 4b shows the breakup and rubble of the ceramic material at the edges of the penetration cavity. The virtual sectioned surfaces in figures 4c–f are ~2.2, 6.7, 11.2, and 15.7 mm from the front face of the specimen, respectively. The increasing amount of damage around the penetration cavity, with increasing distance from the front face, is readily apparent.

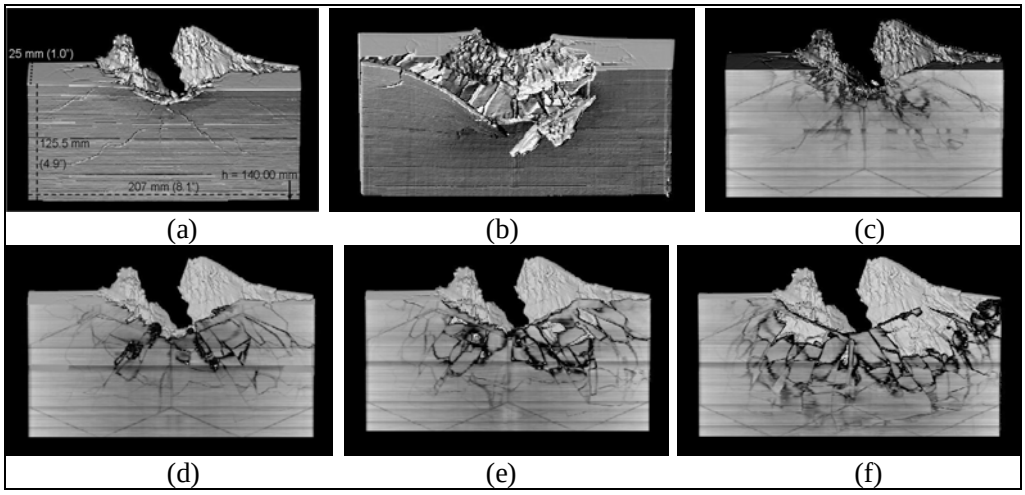

Figure 4. A series of 3-D solid visualization images with material removed from the front face towards the back face: (a) front (impact) side, (b) back (exit) side, and (c–f) front view with 2.2, 6.7, 11.2, and 15.7 mm of material removed, respectively.

Damage is visible relatively far from the penetration cavity at about 140 mm high and at the through-thickness distance of 15.7 mm (figure 4f). These 3-D solid images and the individual CT images they were created from are indicative of the failure of the ceramic material and encapsulation at the back side of the specimen relatively far from the penetration cavity before the specimen was completely penetrated.

The view in figure 5 is looking at the side of the specimen rotated to the right so that the front of it is on the left. The bottom part of the entrance hole of the penetration cavity is near the top of the images in the front face. The virtual sectioned surfaces in figures 5a–h are ~9.9, 19.7, 29.6, 39.5, 59.7, 69.6, 90.7, and 125.3 mm from the side of the specimen, respectively. It can be clearly seen how ceramic material cracked and broke away with the case in the back right area

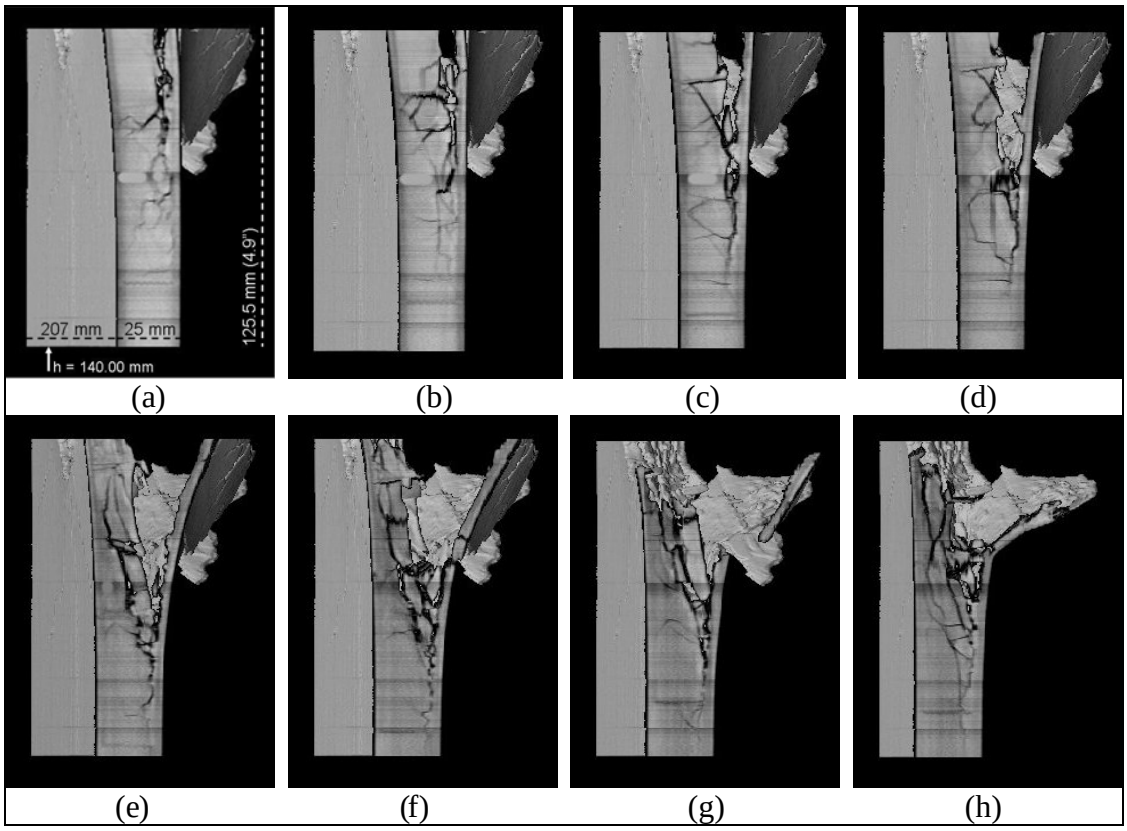

Figure 5. A series of 3-D solid visualization images with material removed perpendicular to the faces from the right side as viewed from the front: (a–h) view looking at the front and side with 9.9, 19.7, 29.6, 39.5, 59.7, 69.6, 90.7, and 125.3 mm of material removed, respectively.

(impact view) around the penetration cavity. The surface at 90.7 mm (figure 5g) is about at the center of the penetration cavity, and the surface at 125.3 mm (figure 5h) is at the other side of the penetration cavity. Secondly, damage is visible relatively far from the penetration cavity towards the back of the specimen (right side) at about 140 mm high, which is at the bottom of the images in figures 5e–h.

6.3 Three-Dimensional Point Cloud and Surface Visualization

A 3-D point cloud is a set of points in space that define geometrical characteristics (i.e., shape, size, and location) of a specimen or scanned volume and features within. Location of the points is determined by appropriate (image) segmentation of the feature or features of interest. Figure 6 is a point cloud of the hole in the front of the panel, as defined by the DR (figure 2b), with a circle fit for diameter. The diameter of the entrance hole is 58.40 mm, with the center 282.00 mm high.

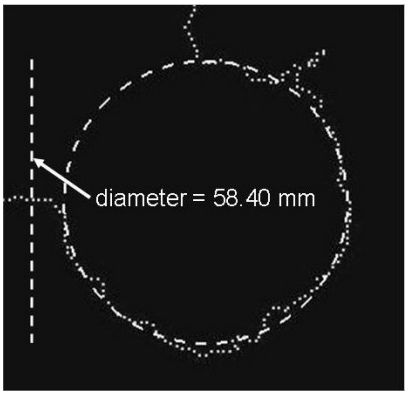

Figure 6. Point cloud of entrance hole with a circle fit for diameter.

Figure 7 is a point cloud of the overall damage and back face of the specimen in the second overlapping set of scans. The view is looking at the front of the specimen tilted forward 50° from a perpendicular line of sight. The back face is the flat-looking area of points to the left and right of the middle "bulge," which is at the front of the specimen, and the peeled back rear case (top middle of figure). The points in the bulge include the bowing of the front of the specimen, damage outside of the penetration cavity, and the penetration cavity itself. The presence of damage relatively far from the penetration cavity at the top of the image is shown by the isolated points at the bottom of the image. Also tilted at 50°, figure 8 is a point cloud of the bulge and the damaged case behind it, where the back face and isolated points have been removed (from figure 7).

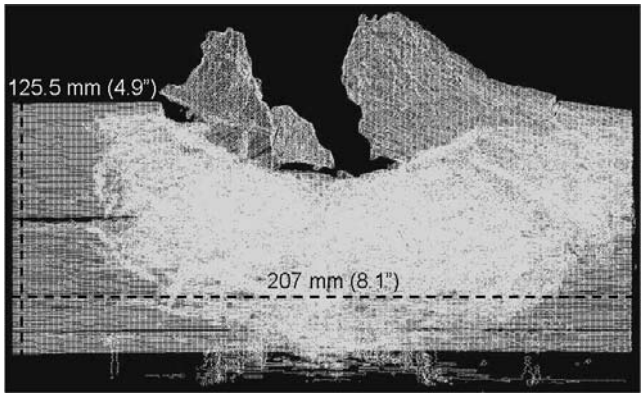

Figure 7. A 3-D point cloud of the overall damage and back face.

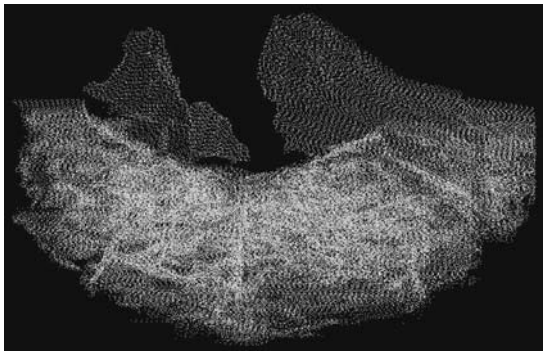

Figure 8. A 3-D point cloud of the front bulge, penetration cavity, and damaged case.

Figure 9 is a point cloud created using only the set of overlapping scans that went through a section of the penetration cavity itself. The top image is looking at the top of the specimen in the negative z (–z) direction. The bottom image shows only the walls of the cavity that are tilted into the page relative to the top down view in the top image. Free-form 3-D surfaces (non-uniform rational basis/bezier spline [NURBS] method [*14*, *15*]) were fit to the cavity wall point clouds. These are shown by the wavy surfaces passing through the points on either side of the section of penetration cavity in figures 10 and 11, which are isometric views from rear side and impact side perspectives, respectively, including all of the points showing the specimen edges. Although these surfaces follow the section of penetration cavity quite well, it is useful to take a simpler and more direct informative approach of fitting planes to these point clouds. The fit planes (NURBS) are shown in figures 12 and 13, which are also isometric views from rear side and impact side perspectives, including all of the points. The tilt of the two planes defining the section of penetration cavity can be seen more easily than the general behavior of the free-form surfaces. The internal angle between the two planes in the physical x-y plane (CT scan plane) is about 125°.

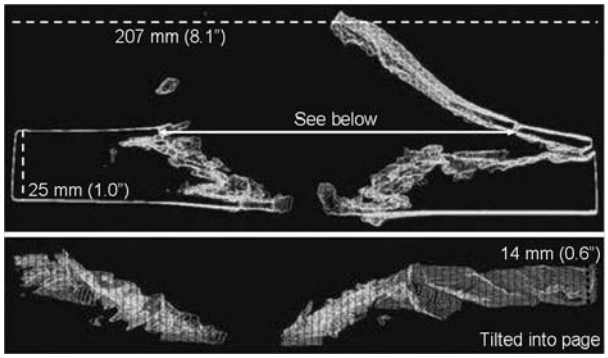

Figure 9. A 3-D point cloud of the section of the penetration cavity.

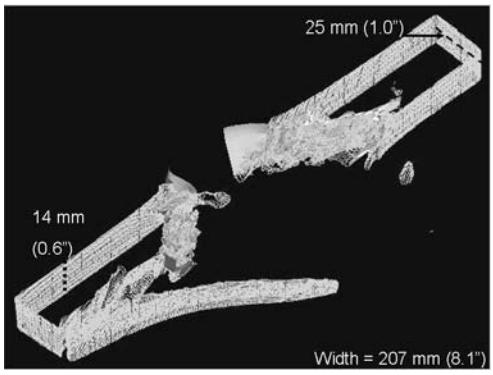

Figure 10. Point cloud of cavity section with fit free-form surfaces (NURBS): rear perspective.

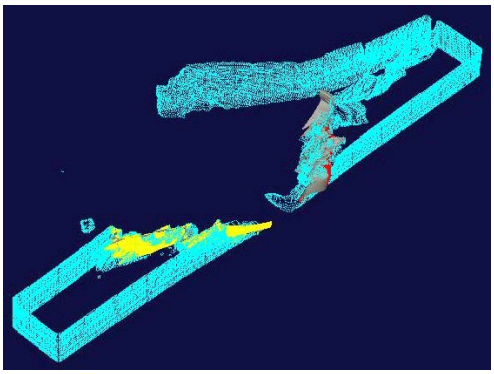

Figure 11. Point cloud of cavity section with fit free-form surfaces (NURBS): impact perspective.

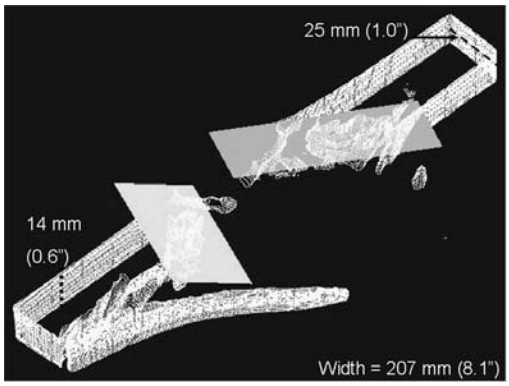

Figure 12. Point cloud of cavity section with fit planar surfaces (NURBS): rear perspective.

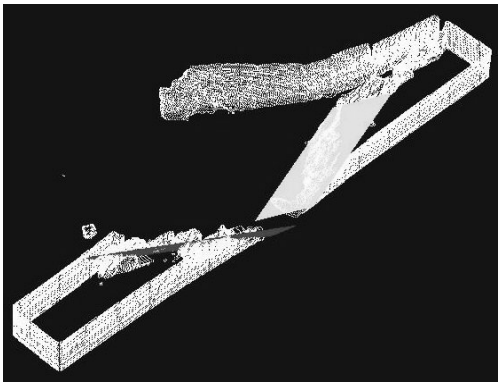

Figure 13. Point cloud of cavity section with fit planar surfaces (NURBS): impact perspective.

The equations (millimeters) of the left and right planar surfaces in figure 13 (impact side perspective) are as follows:

$$.437x + .674y + .595z - 136 = 0 \text{ (Left)}, \tag{1}$$

and

$$-.47x + .608y + .639z - 147 = 0 \text{ (Right)}, \tag{2}$$

which can be written as

$$x_L = -1.54y - 1.36z + 311, \tag{3}$$

and

$$x_R = 1.29y + 1.36z - 313. \tag{4}$$

Table 1 gives the data set of $\{z, y_n, x_{nL}, x_{nR}\}$ for five values of z (vertical position) within the penetration cavity starting near the bottom of the cavity, where three values of y (n = 3) were chosen spanning the through-thickness depth (+y direction) of the cavity. The $\{x_{nL}, y_n, z\}$ and $\{x_{nR}, y_n, z)$ points give the approximate location of the walls of the section of the cavity and provide the fitting data to generate a representative penetration cone surface. Figure 14 shows isometric views from an impact side perspective of the fit penetration cone relative to segmented point cloud representations of selected CT scans, which show the boundaries of the damaged specimen. The penetration cone has an internal angle of 121.9° and an upward tilt out of the x-y plane of 34°. The surface of the cone is mesh shaded in figure 14a in order to maximize the visibility of the points in the vicinity of the penetration cavity. The cone is shaded with an opaque surface in figure 14b in order to emphasize the location, angle, and tilt of the cavity within the damaged structure of the specimen.

Table 1. Data points {z, y_n, x_{nL}, x_{nR}} on fit planar surfaces.

z Position (mm)	**y_1 Position (mm)**	**y_2 Position (mm)**	**y_3 Position (mm)**	**x_{1L} Position (mm)**	**x_{1R} Position (mm)**	**x_{2L} Position (mm)**	**x_{2R} Position (mm)**	**x_{3L} Position (mm)**	**x_{3R} Position (mm)**
251.60	–15.70	0.00	15.70	–7.14	8.99	–31.35	29.30	–55.57	49.61
255.10	–15.70	0.00	15.70	–11.91	13.75	–36.12	34.06	–60.33	54.37
258.60	–15.70	0.00	15.70	–16.67	18.51	–40.89	38.82	–65.10	59.13
262.10	–15.70	0.00	15.70	–21.44	23.27	–45.65	43.58	–69.87	63.89
265.55	–15.70	0.00	15.70	–26.13	27.96	–50.35	48.27	–74.56	68.58

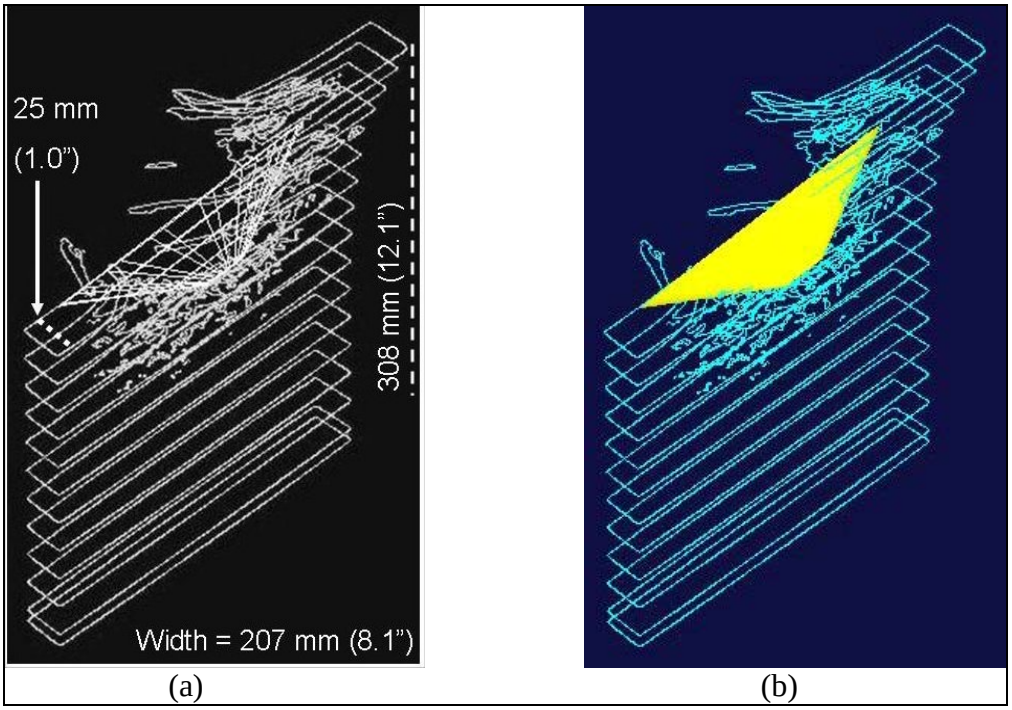

Figure 14. Isometric impact side views of fit cone characterizing entire penetration cavity and selective bottom-to-top CT scans of the specimen that has been (gray scale) segmented and converted to point cloud representations to show the outer boundaries. The penetration cone has an internal angle of 121.9° and an upwards tilt out of the x-y plane (CT scan plane) of 34°.

7. Evaluation of As-Fabricated and Sectioned Specimen (Specimen 2)

7.1 Ultrasonic Scans

Figure 15 shows two through-thickness amplitude difference C-scan images gated to show the bulk characteristics of the specimen and taken using 5- (figure 15a) and 10-MHz (figure 15b) columnar immersion transducers. The sectioned side of the specimen is on the right, and the

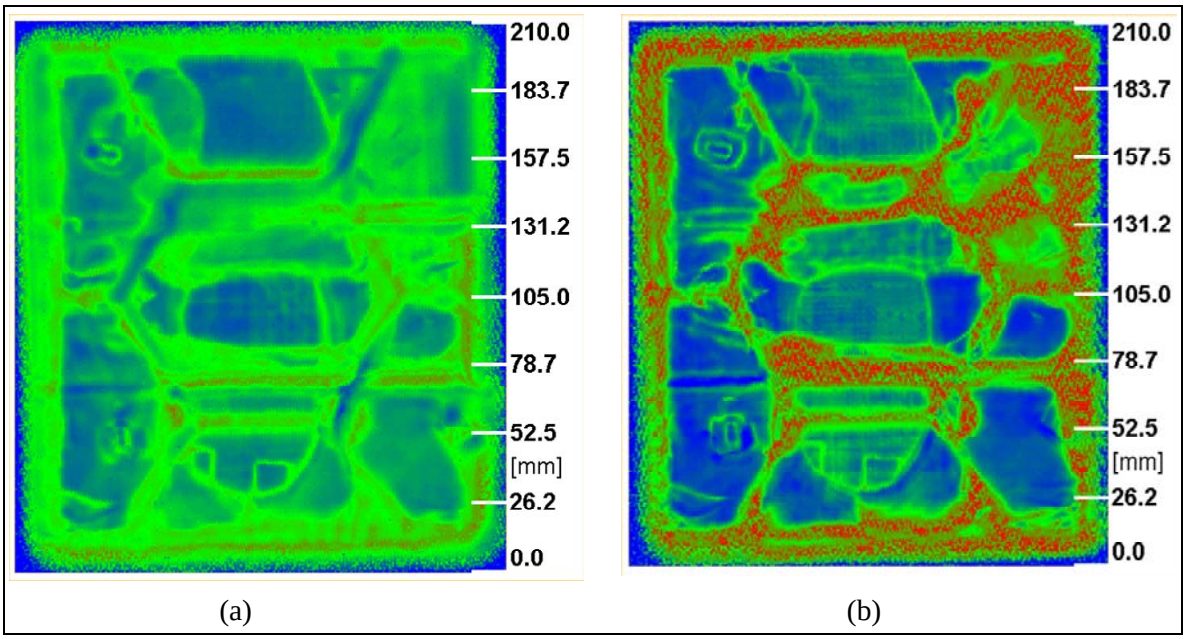

Figure 15. Through-thickness amplitude difference C-scan images of the specimen, both gated to show bulk characteristics and taken using (a) 5- and (b) 10-MHz immersion transducers. The scale is given in order to provide the location of CT scans above the bottom of the specimen for comparison to the areal C-scans.

long vertical dimension (210 mm) is labeled. The up direction from the bottom of the images towards 210 mm corresponds to increasing z in the CT scans of the specimen. Blue and red represent the least and most attenuation (signal loss), respectively. The two-toned green and red band around the perimeter of the specimen is caused by edge-effect attenuation. The pattern of the tile layout can be clearly seen as well as two spacers in the left-hand side of the specimen, especially in figure 15b. Figure 15a shows that there is some significant attenuation over most of the specimen. Figure 15b shows a number of individual features, including a double-lobe shaped area of varying attenuation down the center of the specimen starting at about 28 mm from the bottom. Figure 15b also shows two horizontal bands of higher attenuation vertically centered at about 74 and 143 mm from the bottom of the specimen. The lower band extends from the left-hand side of the middle tile in its bottom area to the right-hand side of the specimen. The upper band is mostly in the top area of the middle tile, with a small portion in the lower area of the top middle (partial) tile. The entire area of the top right (partial) tile is relatively highly attenuated.

7.2 CT Scans

Figure 16 shows a series of CT scans (images) of the specimen at vertical positions of 80.00, 105.00, 111.40, 126.80, 144.80, 148.40, 165.00, 194.60, 195.50, 204.5, 225.00, and 240.00 mm (figures 16a–l). The front of the specimen is at the top of the images. The darker vertical bands in the images are indications of the area between adjacent tiles. The very faint concentric rings featured in the center of the images is an image artifact due to using relatively narrow image windowing to increase contrast; it is not an indication of a real physical feature in the specimen.

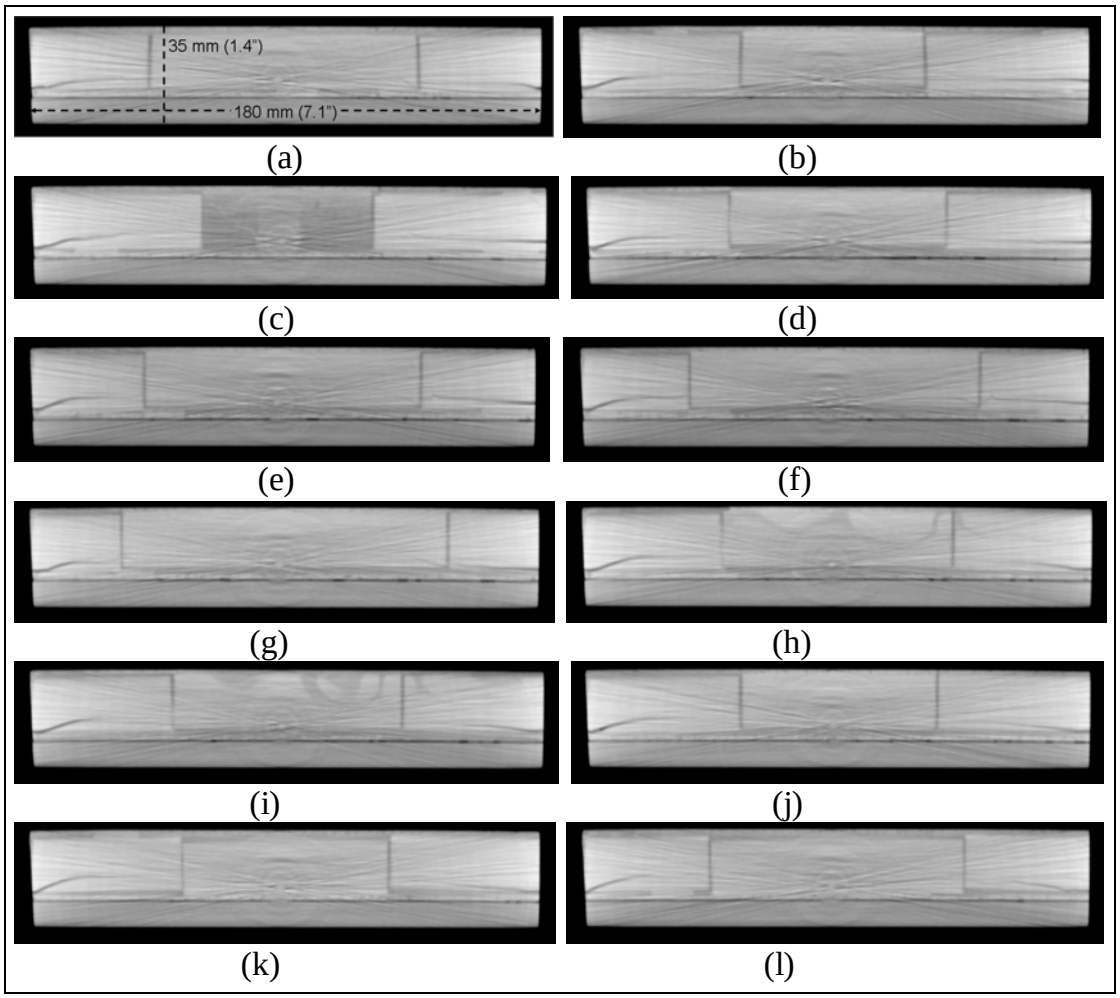

Figure 16. A series of cross-sectional CT scans (images). Scans (a–l) were ~26, 51, 57, 73, 91, 94, 111, 141, 142, 150, 171, and 186 mm above the bottom of the specimen, respectively.

From the lowest to the highest scan, they were ~26, 51, 57, 73, 91, 94, 111, 141, 142, 150, 171, and 186 mm above the bottom of the specimen, respectively, which is at the bottom of the scans in figure 15. The sectioned side of the specimen is on the right as it is for the ultrasonic scans. Cracking is evident in the sectioned side of the specimen as well as in the left side of the specimen.

The scan at 26 mm (figure 16a) shows the cracking in both sides of the specimen and a faint indication of cracking in the bottom right area of the center tile, which has fair correlation with the C-scan image in figure 15b. The scan at 51 mm (figure 16b) shows a horizontal band of lower density material below the middle tile. This is a few millimeters below the top of the bottom middle tile in the C-scans, which is in the area of the double-lobe shaped feature. The entire middle tile area has a lower density in the scan at 57 mm (figure 16c), which corresponds to the horizontal region between the middle and bottom middle tiles in the C-scans. Lower density horizontal bands are also apparent below the middle and right tiles of the scan at 73 mm

(figure 16d), which correlates well with the higher attenuation region centered at about 74 mm in the C-scans. The scans at 91 (figure 16e) and 94 mm (figure 16f) both show low-density bands below portions of the middle and right tiles and the cracking in the sectioned side of the specimen extending into the middle tile. The scan at 94 mm, which appears to have a slightly lower density band than the scan at 91 mm, is near the top of the bottom right tile in the C-scans. The scan at 111 mm (figure 16g) shows lower density bands below the middle and right tiles, with similar thickness and a somewhat faint short linear feature starting at the bottom right corner of the middle tile just above the low density band. This probably indicates that the cracking in the sectioned side of the specimen extends into the middle tile in this scan also.

This correlates well with the higher attenuation region just above the center of the middle tile and the region to its right in the C-scans. The crack in the left side of the specimen also appears to reach the middle tile. There is some indication of the extended crack in the left side of the specimen near the bottom of the top left tile in the C-scans. The scans at 141 (figure 16h) and 142 mm (figure 16i) show wavy and nonuniform regions of low density, respectively, near the front (top) of the middle tile that extend into the right tile. This correlates well with the higher attenuation region centered at about 143 mm in the C-scans. The low-density feature below the middle tile in the scan at 150 mm (figure 16j) appears to extend into the tiles on each side. This is in the vicinity of the top of the middle tile in the C-scans, which is in fair correlation. The scans at 171 (figure 16k) and 186 mm (figure 16l) both show low-density bands below the left and right tiles, with the wider band below the right tile, which is the sectioned side of the specimen. Both scans also show a low-density band above the middle tile that appears to be wider in these scans than in the other scans. These scans seem to have a better correlation with the C-scan in figure 15a than the one in figure 15b. The scan at 186 mm also shows a crack in the bottom right corner of the middle tile. This particular feature correlates well with the higher attenuation region that forms a protrusion out of the upper portion of the top right tile into the top middle tile in the C-scan in figure 15b. Considering all the CT scans, it is apparent that the C-scans were not very sensitive to portions of cracks at or near the specimens' edges, likely due to the ultrasonic edge effect attenuation.

8. Conclusions

A wide range of ballistic damage in a sectioned encapsulated ceramic panel specimen including complete penetration was scanned and extensively characterized using XCT 2-D cross-sectional (planar) and 3-D volumetric analysis. Several damage features were captured and discussed, including low severity ceramic cracking relatively far from the penetration cavity, ceramic cracking, fragmentation, and rubble, encapsulation cracking and exit (rear) side peel back, impact (front) face bulging, and penetration cavity size and geometry. Successive application of XCT 2-D evaluation, volumetric solid visualization and analysis, and volumetric point cloud

visualization and derived feature surface analysis provided extensive and important qualitative and quantitative data about damage features. Characteristics of captured damage features provided better understanding of the physical processes of damage initiation and growth.

Several features in a different sectioned, nonimpacted, and encapsulated ceramic panel specimen were characterized using UT and XCT, including cracking that may have been caused by the physical sectioning process. Ultrasonic amplitude difference C-scans through the thickness of the specimen showed a number of attenuation features, including wide bands and regions over large areas of tiles of higher attenuation. XCT scans showed a number of spatial features located in 3-D space, including cracks in the edges of tiles extending further into the interior and low-density regions. The ultrasonic bulk C-scans and through-thickness spatial XCT scans had a fairly good correlation, with a number of matching features. The XCT and UT methods were able to synergistically provide comprehensive and detailed information about the internal geometrical and physical characteristics of the panel specimen.

9. References

1. Green, W.; Miller, H.; LaSalvia, J.; Dandekar, D.; Casem, D. Evaluation of Ballistically-Induced Damage in Ceramic Targets by X-ray Computed Tomography. *Proceedings of the 32nd International Conference on Advanced Ceramics and Composites - Topics in Ceramic Armor*, Daytona Beach, FL, 27 January–1 February 2008.

2. Green, W.; Rupert, N.; Wells, J. Inroads in the Non-invasive Diagnostics of Ballistic Impact Damage. *Proceedings of the 25th Army Science Conference*, Orlando, FL, 27–30 November 2006.

3. Miller, H.; Green, W.; LaSalvia, J. Ballistically-Induced Damage in Ceramic Targets as Revealed by X-ray Computed Tomography. *Proceedings of the 31st International Conference on Advanced Ceramics and Composites - Topics in Ceramic Armor*, Daytona Beach, FL, 21–26 January 2007.

4. Bourne, N.; Green, W.; Dandekar, D. On the One-dimensional Recovery and Microstructural Evaluation of Shocked Alumina. *Proceedings of the Royal Society A: Mathematical, Physical, and Engineering Sciences;* published online: doi:10.1098 /rspa.2006.1713, United Kingdom, 2006.

5. Wells, J.; Green, W.; Rupert, N.; MacKenzie, D. Capturing Ballistic Damage as a Function of Impact Velocity in SiC-N Ceramic Targets. *Proceedings of the 30th International Conference on Advanced Ceramics and Composites - Advances in Ceramic Armor*, Daytona Beach, FL, 2006.

6. Green, W.; Carter, R. Evaluation of Ballistic Damage in an Encapsulated Ceramic Panel via X-ray Computed Tomography. *Proceedings of Review of Progress in Quantitative NDE*, Chicago, IL, 20–25 July 2008; Vol. 28B, pp 1099–1106.

7. Newton, T. H.; Potts, D. G., Eds. Technical Aspects of Computed Tomography. In *Radiology of the Skull and Brain*; Vol. 5, The C. V. Mosby Company: St. Louis, MO, 1981.

8. American Society for Testing and Materials (ASTM). *Standard Practice for Computed Tomographic (CT) Examination*, Designation: E 1570-95a, Columbus, OH, 1995.

9. Dennis, M. J. Industrial Computed Tomography. In *Nondestructive Evaluation and Quality Control*; Vol. 17, American Society for Metals (ASM) International, ASM Handbook, 1989.

10. Stanley, J. H. Physical and Mathematical Basis of CT Imaging, American Society for Testing and Materials (ASTM), ASTM CT Standardization Committee (E7.01.07), ASTM Tutorial: Section 3, Columbus, OH, 1986.

11. Mix, P. E. *Introduction to Nondestructive Testing*; John Wiley & Sons: New York, 1987; pp 104–153.

12. Krautkramer, J.; Krautkramer, H. *Ultrasonic Testing of Materials*; Springer-Verlag: New York, 1990.

13. Bhardwaj, M. C. *Ceramic Monographs – Handbook of Ceramics;* Vol. 41, No. 1, 1992.

14. Wikipedia, Nonuniform Rational B-spline. http://en.wikipedia.org/wiki/NURBS (accessed January 2009).

15. SDRC/Imageware. *Basic Reverse Engineering with Surfacer: Training Guide*; Ann Arbor, MI, March 1999; pp 244–245, 326–327.

NO. OF
COPIES ORGANIZATION

1 (PDF only) DEFENSE TECHNICAL INFORMATION CTR
DTIC OCA
8725 JOHN J KINGMAN RD
STE 0944
FORT BELVOIR VA 22060-6218

1 DIRECTOR
US ARMY RESEARCH LAB
IMNE ALC HRR
2800 POWDER MILL RD
ADELPHI MD 20783-1197

1 DIRECTOR
US ARMY RESEARCH LAB
AMSRD ARL CI OK TL
2800 POWDER MILL RD
ADELPHI MD 20783-1197

1 DIRECTOR
US ARMY RESEARCH LAB
AMSRD ARL CI OK PE
2800 POWDER MILL RD
ADELPHI MD 20783-1197

ABERDEEN PROVING GROUND

1 DIR USARL
AMSRD ARL CI OK TP (BLDG 4600)

NO. OF
COPIES ORGANIZATION

ABERDEEN PROVING GROUND

8 DIR USARL
AMSRD ARL WM MB
R H CARTER
AMSRD ARL WM MD
R BRENNAN
W H GREEN (5 CPS)
J SANDS

INTENTIONALLY LEFT BLANK.